In Vivo Imaging of the Fine Structure of Rhodamine-Labeled Macaque Retinal Ganglion Cells

Daniel C. Gray,[1,2] *Robert Wolfe,*[2] *Bernard P. Gee,*[2] *Drew Scoles,*[2] *Ying Geng,*[1,2] *Benjamin D. Masella,*[1,2] *Alfredo Dubra,*[1] *Sergio Luque,*[3] *David R. Williams,*[1,2] *and William H. Merigan*[1]

Purpose. The extent to which the fine structure of single ganglion cells, such as dendrites and axons, can be resolved in retinal images obtained from the living primate eye was investigated.

Methods. Macaque retinal ganglion cells were labeled with retrograde transport of rhodamine dextran injected into the lateral geniculate nucleus. Fluorescence images of the ganglion cells were obtained in vivo with an adaptive optics scanning laser ophthalmoscope.

Results. Axons and dendritic arborization could be resolved in primate retinal ganglion cells in vivo, comparing favorably in detail with ex vivo confocal images of the same cells. The full width at half maximum of the transverse line spread function (LSF) was 1.6 μm, and that of the axial point spread function (PSF) was 115 μm. The axial positional accuracy of fluorescence- labeled objects was approximately 4 μm.

Conclusions. This in vivo method applied to ganglion cells demonstrates that structures smaller than the somas of typical retinal cells can be accessible in living eyes. Similar approaches may be applied to image other relatively transparent retinal structures, providing a potentially valuable tool for microscopic examination of the normal and diseased living retina. (*Invest Ophthalmol Vis Sci.* 2008;49:467–473) DOI:10.1167/iovs.07-0605

Correction of higher order aberrations of the cornea and lens with adaptive optics (AO) has improved the resolution of images of the living retina to the point where single-cone photoreceptors can be imaged routinely. Recently, several retinal imaging methodologies—flood-illuminated systems,[1] scanning laser ophthalmoscopes,[2] and optical coherence tomography[3]—have incorporated AO, making possible the routine imaging of one retinal cell type, the cone photoreceptor, which offers high contrast. Unfortunately, other neurons in the retina are transparent and, thus, difficult to image. For example, the signal from the ganglion cell layer is 60 times lower than that from cones (Miller D, personal communication, September 2006). The low contrast of the outermost retinal cells, combined with difficulties such as eye movements and light safety limits, makes imaging these cells challenging.

Imaging retinal ganglion cells is of special importance because it offers the possibility of directly observing the function of myelinated, spiking neurons of the central nervous system in the normal and diseased retina. Detailed description of the morphology and physiology of primate ganglion cells have been carried out by Rodieck and Watanabe,[4] Watanabe and Rodieck,[5] and Dacey et al.,[6–9] resulting in the identification of more than 20 different retinal ganglion cell types. The function of primate retinal ganglion cells has received detailed scrutiny recently with the use of in vitro methods (see, for example, Dacey et al.[7]), and these studies must be supplemented by investigations in the living primate. It has been possible to examine the different functional contributions of the parvocellular and magnocellular pathways to vision because they are anatomically segregated in the lateral geniculate nucleus (LGN), allowing psychophysical measurements in monkeys after selective lesioning.[10] However, the functional role of many other retinal ganglion cell types cannot easily be disentangled in this way, prompting the need for a better method to distinguish these cells in the living eye.

In vivo imaging of primate ganglion cell bodies has been previously reported by Cordeiro et al.[11] and Gray et al.,[12] but the detailed structure of dendrites and axons was not resolved in these studies. Several reports have also described imaging labeled retinal ganglion cells in mice and rats using wide-field imaging systems.[11,13–17] None have reported visualization of individual dendrites or axons. Biss et al.[18] used AO combined with fluorescence imaging in the mouse to visualize GFP-labeled microglia and dendritic features, but their technique has not yet been applied to ganglion cells.

In this article we show that individual ganglion cell axons and dendrites can be imaged in live macaque monkeys. By analyzing the transverse and axial response of these high-contrast fluorescence-labeled neurons, we were able to characterize the resolution of the in vivo imaging system. In addition, we confirm the identity of in vivo imaged cells by comparing them directly with ex vivo images of the same tissue obtained with a high numerical aperture (NA) microscope objective.

Methods

Injections

A three-dimensional grid of 0.5-μL injections at 2-mm intervals of rhodamine fluorescent dye (dextran, tetramethylrhodamine, and biotin; 3000 MWt, lysine fixable; Molecular Probes, Eugene, OR) was made stereotactically into the right and the left LGN of two *Macaca*

From the [1]Center for Visual Science and [2]Institute of Optics, University of Rochester, Rochester, New York; and the [3]Centro de Desarrollo de Sensores, Instrumentación y Sistemas, Universidad Politécnica de Cataluña, Terrassa, Spain.

Supported in part by the National Science Foundation Science and Technology Center for Adaptive Optics, managed by the University of California at Santa Cruz under cooperative agreement NSF Grant cfao-ast-9876783. Additional support was provided by Bausch and Lomb, Inc.; National Institutes of Health Grant BRP-EY014375, Training Grant EY07125, and Core Grant EY001319; and grants from Research to Prevent Blindness.

Submitted for publication May 23, 2007; revised August 27, 2007; accepted November 14, 2007.

Disclosure: **D.C. Gray**, Optos (P, E); **R. Wolfe**, None; **B.P. Gee**, None; **D. Scoles**, None; **Y. Geng**, None; **B.D. Masella**, None; **A. Dubra**, P; **S. Luque**, None; **D.R. Williams**, Bausch and Lomb Inc. (F), Optos (C, P); **W.H. Merigan**, None

Presented at the annual meeting of the Association for Research in Vision and Ophthalmology, Fort Lauderdale, Florida, May 2007.

The publication costs of this article were defrayed in part by page charge payment. This article must therefore be marked "*advertisement*" in accordance with 18 U.S.C. §1734 solely to indicate this fact.

Corresponding author: Daniel C. Gray, Optos Plc, Queensferry House, Carnegie Business Campus, Queensferry Road, Dunfermline, Fife KY11 8GR, UK; dgray@optos.com.

mulatta monkeys. Thirty-six penetrations were made in monkey 1, and 18 penetrations were made in monkey 2. Three injections were made at each penetration. Injections were made with a 25-μL Hamilton syringe through a length of 32-gauge hypodermic tubing.

In Vivo Imaging

The fluorescence adaptive optics scanning laser ophthalmoscope (AOSLO), monkey imaging methods, and postprocessing methods have been described.[12] For in vivo imaging, the monkeys were anesthetized with isoflurane, and the dosage was modulated to control eye drift. Monkey retinas were imaged in vivo with the AO system 4 days and 7 days after the LGN injection for monkey 1 and 4 and 6 days for monkey 2. Axial lengths of the injected eyes were measured with an IOLMaster (Carl Zeiss Meditec, Jena, Germany) and were used to calculate transverse and axial retinal distances. The Elmsley model eye was used to convert diopters of focus to axial distance using the following formula: μm focus = $\frac{4}{3}$\{1/[power(D) + focus(D)] − 1/power(D)\} × 10^6, where the power in diopters has been calculated by linearly scaling eye size by the measured axial length. Over a 6-mm entrance pupil diameter, the equivalent NA was between 0.229 and 0.238, compared with 0.18 for a typical human eye. Each monkey was fitted with a rigid, gas-permeable contact lens to reduce astigmatism and defocus. Standard ophthalmic trial lenses were used to correct residual astigmatism and defocus to values that could be corrected with the deformable mirror (typically <0.75 μm root mean square (RMS) over a 5.8- to 6.1-mm pupil in both monkeys). The images in monkeys 1 and 2 were taken at eccentricities of approximately 20° to 30°, where ganglion cell dendrites are typically larger and have wider branching patterns than locations closer to the fovea. Because of the weak fluorescence signal from the retina, 400 to 1000 raw video frames were dual registered and averaged using methods described in Gray et al.[12] Fluorescence videos were acquired with confocal pinhole diameters of 6.2 μm and 9.3 μm at the retina or 3.97 and 5.95 Airy disc radii. All experimental protocols were approved by the University Committee of Animal Resources at the University of Rochester Medical Center, complied with the Public Health Service policy on Humane Care and Use of Laboratory Animals, and adhered to the ARVO Statement for the Use of Animals in Ophthalmic and Vision Research.

Ganglion cell dendrites and axons were visualized by producing a photodynamic enhancement of rhodamine fluorescence similar to that described in vitro by Dacey et al.[7] and earlier used by the authors to image ganglion cell bodies in vivo.[12] Retinal areas were selected for detailed imaging on the basis of their susceptibility to fluorescence enhancement. The scan field size was restricted to 1° or 2° to concentrate the argon-krypton laser tuned to 530 nm on a chosen area. Average light exposure was 100 to 130 μW entering the pupil of the eye. Each location was then exposed for up to 5 minutes to gauge whether photo-filling would be observed with continued light exposure. Only some locations exhibited brightening; areas that did not were presumed not to contain high enough concentrations of dye.

Axial-Resolution Measurements and Data Processing

Measurements of axial resolution were made with 18 focus steps at 7.12-μm increments over a range of 120 to 130 μm. The confocal pinhole was 5.95 Airy disc radii, and the photomultiplier tube (PMT) gain was set to ensure no pixel saturation. The image stack was normalized by the maximum pixel value contained in the entire set. The image stack was then imported into NIH ImageJ (free software from NIH for image processing[11]), and subpixel registration with a pyramid alignment approach was applied using a plug-in (Turbo Reg; free software plug-in for NIH ImageJ, available from the Biomedical Imaging Group, Swiss Federal Institute of Technology Lausanne; http://bigwww.epfl.ch/thevenaz/turboreg/[19]) on a subregion of the image. Axial profiles of ganglion cell bodies were measured as the average intensity within a central area of the cell.

To reduce noise in the measurement, the raw in vivo data were fit with a least squares method to a theoretical diffraction-limited axial intensity profile. The full width at half maximum (FWHM) of the fit was used as a measure of axial resolution. The theoretical three-dimensional point spread function (PSF) was calculated by modeling the instrument as an incoherent confocal imaging system (mathematical framework established by Wilson[20,21]). The intensity response as a function of the object position (x_s, y_s, u_s), of a spherical ganglion cell body was then calculated by the convolution of the intensity PSF with the ganglion cell and confocal pinhole using the following equation:

$$I_{ganglion\ cell}(x_s, y_s, u_s) = \int_{\pm\infty}\int \int_{\pm\infty}\int |h_1(x_1, y_1, u_1)|^2 \times \varepsilon_1(x_1 - x_s, y_1 - y_s, u_1 - u_s)|h_2(x_2 - x_1, y_2 - y_1)|^2 \times dx_1 dy_1 du_1 \times p(x_2, y_2)dx_2 dy_2$$

where x and y are transverse dimensions, and u is the axial dimension, (h_1) is the input PSF, (ε_1) is the intensity distribution of the object, (h_2) is the outgoing PSF (identical with (h_1) for in vivo imaging), and (p) is the transmission function of the confocal pinhole.

Ex Vivo Imaging

After in vivo imaging, the two monkeys were humanely killed for histologic analysis within 1 hour of the end of imaging on the final day. Under deep anesthesia, both monkeys were perfused, initially with 2 L saline, to flush blood from the vascular system and then with 4% paraformaldehyde. The eyes were fixed further in the eyecup for an additional 40 minutes. Then the retinas were removed, placed as wholemounts on slides, covered in mounting medium (Vectashield; Vector Laboratories, Burlingame, CA) to minimize fading of fluorescence, and coverslipped. The ex vivo tissue was then imaged on a confocal microscope (Olympus; Tokyo, Japan). Corresponding focus stacks were taken at the locations imaged in vivo with 10× (0.3 NA), and 40× (0.85 NA) microscope objectives (nonimmersion) permitting direct comparison to the in vivo tissue. The 0.3-NA images were obtained with microscope settings that approximated the imaging parameters obtained in vivo. Zoom and pixel spacing was adjusted close to the in vivo parameters. A pinhole size of 4.62 Airy disc radii was the closest match to the pinhole used for the in vivo data, 3.97 Airy disc radii.

Results

Adaptive Optics Florescence Imaging

Fluorescence enhancement was most dramatic on day 4 and was slightly diminished by day 6 (monkey 2) or 7 (monkey 1). Figure 1 demonstrates the photofilling effect in monkey 1 on day 4 after the injection. An increase in brightness was observed, as reported by Dacey et al.[7]

Cell bodies were visible without AO (Figure 2a), but dendrites and axons were only fully resolved when the AO was activated (Fig. 2b). The insets in Figures 2a and 2b show a cross-section along the white line demonstrating that, without AO, fine dendrites cannot be distinguished from neighboring dendrites. With AO activated, however, those dendrites were resolvable. Figures 2c and 2d show the same images as seen in Figures 2a and b2, but contrast was increased to reveal the finer structures. The insets in Figures 2c and 2d show portions of the grayscale histogram of Figures 2a and 2b with a mean value improvement of two times. In monkey 1, an intensity improvement of 1.8 times was measured, but that was a conservative measurement because it was necessary to saturate some pixels representing cell bodies to visualize axonal and dendritic structure.

Figure 3a shows a comparison of the radial averaged power spectral density of Figures 2a (gray) and 2b (black) on a log scale versus spatial frequency. An overall increase in signal resulting from the AO correction was observed from the offset

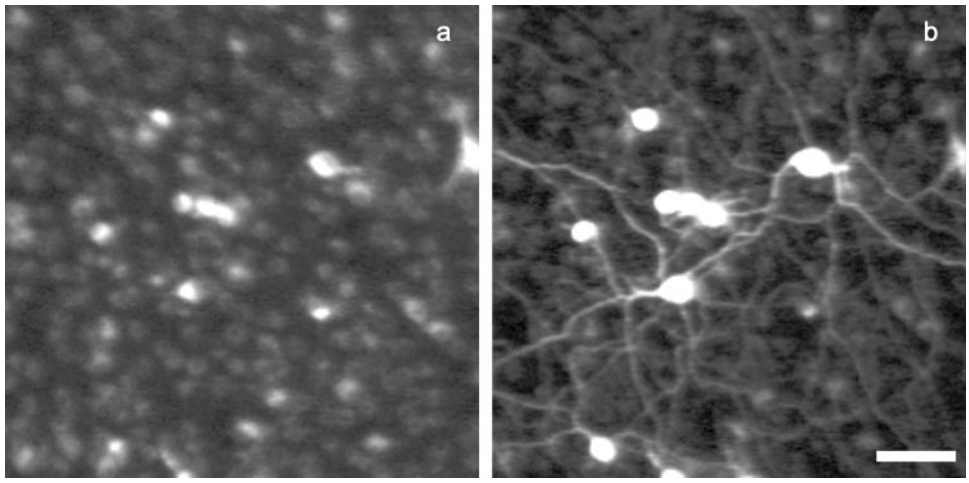

FIGURE 1. (**a**) Before photofilling. (**b**) After photofilling. Both images are an average of 1000 raw video frames and were acquired with AO. The normalized images have been contrast enhanced identically for display purposes. Scale bar, 50 μm.

difference between the AO on (black) and off (gray) plot. Figure 3b shows the ratio of the power spectral density with AO on to that with AO off. At this wavelength and NA, the maximum theoretical spatial frequency that could be imaged in the eye was approximately 140 cyc/deg. The pixel spacing of the instrument was 512 over a 2° field of view for this image, resulting in a 128-cyc/deg limit. Axons and dendrites range in size from less than 1 μm (220 cyc/deg) to several microns. Figure 3b shows a spatial frequency improvement of 19 times at 25 cyc/deg corresponding to 8.9 μm, the approximate diameter of a ganglion cell. In general, the spatial frequency improvement depends on the aberrations of the eye and the spatial frequency content of the object.

Characterization of In Vivo Imaging Performance: Transverse Resolution

The average transverse cross-section across an isolated axon was used as a measurement of the transverse LSF of the in vivo imaging system (shown in Fig. 4a). In Figure 4c, profile mea-

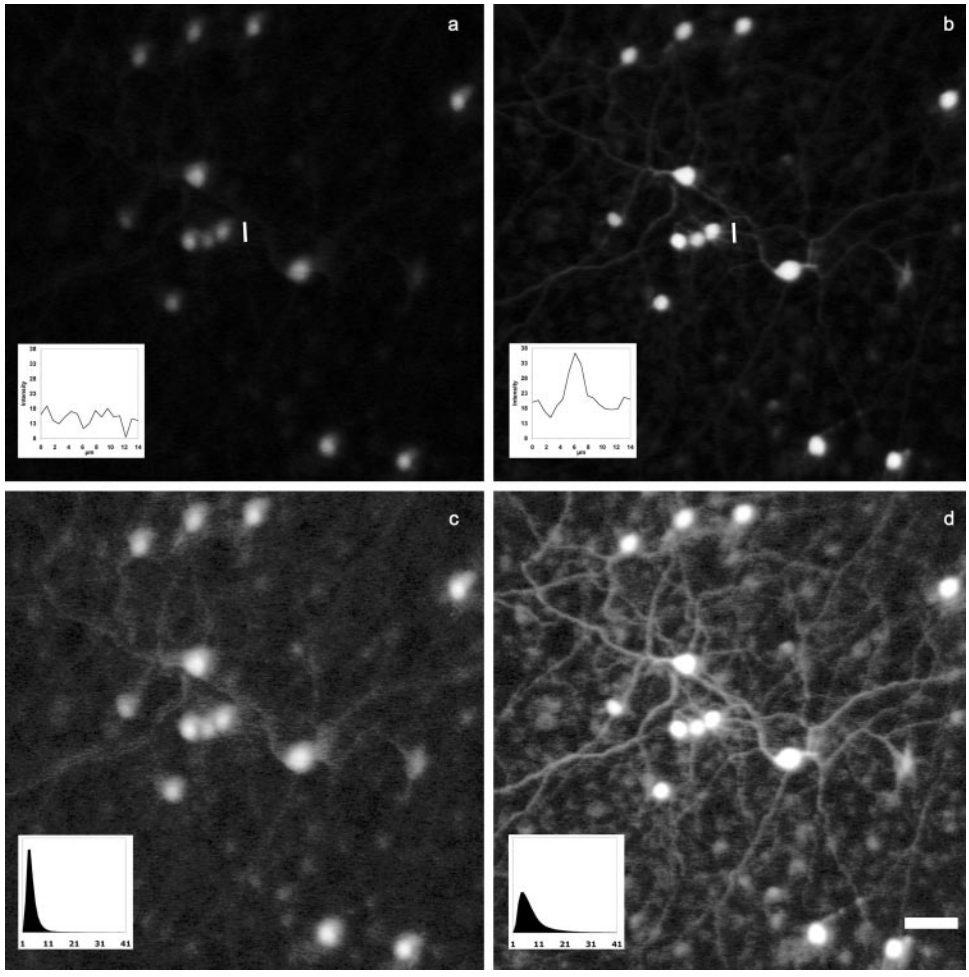

FIGURE 2. Demonstration of the improvement resulting from AO in monkey 1. (**a**) Without AO. (**b**) With AO. The intensity of (**a**) is normalized to the maximum value of (**b**). (**a**, **b**, *insets*) Intensity profile along the *white line*, demonstrating the improvement resulting from AO correction. An RMS wavefront error of 0.375 μm was measured over a 5.8-mm pupil with AO correction OFF and a 0.05-μm RMS error with the AO correction ON. (**c**, **d**) Identically contrast enhanced to increase the visibility of the fine structure. (**c**, **d**, *insets*) Grayscale histograms of (**a**) and (**b**). Original images are registered sums of 400 frames each from the same raw movie; the first half had AO OFF, and the second half had AO ON. Scale bar, 50 μm.

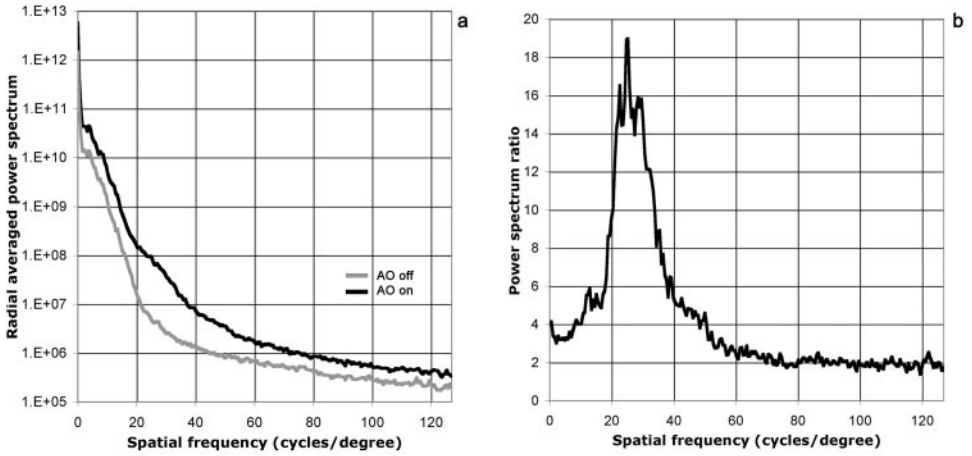

FIGURE 3. (**a**) Radial averaged power spectrum of Figure 2a (*gray*) and Figure 2b (*black*) on a log scale. (**b**) Power spectrum ratio of Figure 2b to 2a.

surements across the same axon, imaged ex vivo (Fig. 4b), show how the axon is smaller than the expected in vivo LSF and, thus, is a good approximation of a line source (axon widths of less than 1 μm yield LSF widths of 5% to 10% larger than a line object). The data were interpolated with a spline fit and normalized (Figs. 4c, 4d). For comparison, the expected normalized LSF and PSF for a diffraction-limited eye with a 0.23 NA have also been plotted (solid and dashed gray lines). The FWHM of the in vivo axon cross-section is 1.6 μm, 26% larger than the expected 1.18-μm LSF FWHM.

Direct Comparison of In Vivo Images to Ex Vivo Images

Figure 5 shows a comparison of in vivo and *ex vivo* images from two locations in monkey 1. The image comparison shows how the in vivo transverse resolution is fine enough to recover most of the dendritic structure. Figure 5a shows an area in which two ganglion cell types can be distinguished in vivo. The lower cell (Fig. 5a, large arrow) has large branching dendrites (greater than 200 μm) whereas the cell immediately above it (Fig. 5a, small arrow) has a narrowly confined dendritic arbor with a mean diameter of 20 μm. The image was taken at approximately 12.5° eccentricity, or 2.78 mm from the fovea, and the 20-μm dendritic field suggests that this is a midget ganglion cell. At this eccentricity, a single primary dendrite branching into many fine dendrites (Fig. 5c, arrow) is morphologically unique to midget cells.[5]

Characterization of In Vivo Axial Resolution

The axial resolution of the stand-alone imaging system has been characterized using a the axial response of a planar mirror surface[22] with an aberration-corrected model eye. The axial resolution of the imaging system is 25% poorer than the expected theoretical resolution. The axial FWHM of 22 ganglion cell bodies was measured to characterize the in vivo axial resolution, and it was found that the average value was 115 μm. This compares well against the experimental limit of 106 μm measured with a model eye (25% higher than the theoretical limit for the same NA).

Characterization of the Positional Accuracy

The axial resolution of an in vivo retinal imaging system is important in reflected light imaging when there are many layers of tissue. However, when objects of interest are sparsely distributed and confined to a narrow axial region of tissue, the

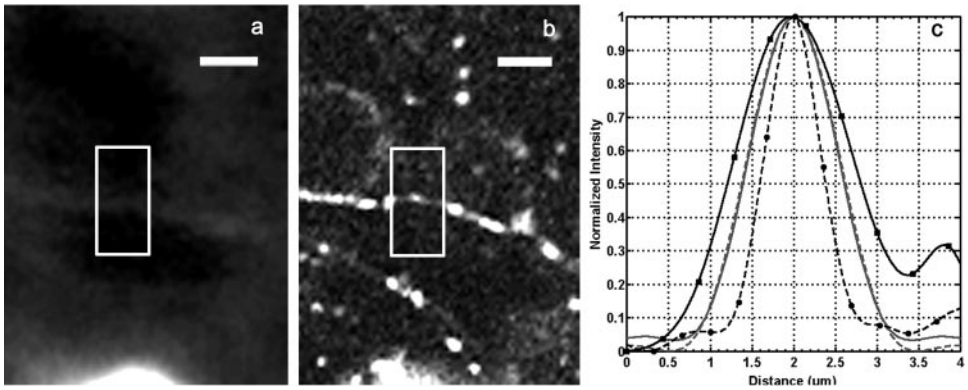

FIGURE 4. Transverse line spread function measurement. (**a**, **b**) In vivo image and corresponding ex vivo image (taken with a 0.85 NA objective) of an isolated axon in monkey 1. Average cross-sections were measured across an axon within the zone marked in *white*. Scale bars, 5 μm. Images have been rescaled and contrast enhanced for display purposes only. (**c**) Plots of the average transverse profile measured from the in vivo and ex vivo data. Square data points are average in vivo measurements. *Solid black line*: spline fit to the in vivo data with FWHM of 1.60 μm. Circular data points are average ex vivo measurements. *Dashed black line*: spline fit to the ex vivo data with FWHM of 0.79 μm. For comparison, in (**c**), the expected theoretical LSF for a 0.23 NA eye is plotted (*solid gray*) with FWHM of 1.18 μm. The theoretical PSF is plotted (*dashed gray*) with FWHM of 1.24 μm.

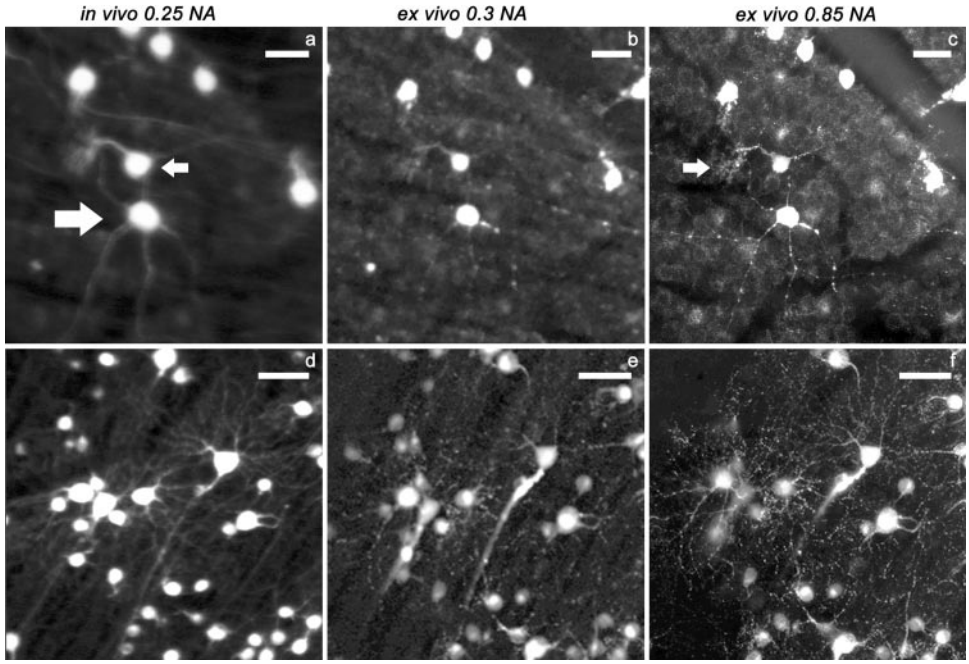

FIGURE 5. Comparison of the in vivo images to the ex vivo images in monkey 1. (**a**, **d**) In vivo images from two retinal locations. (**b**, **e**) Ex vivo images of the same locations made with a low-power (0.3 NA) objective to simulate the NA of the in vivo conditions. (**c**, **f**) Ex vivo images of the same location made with a 0.85 NA objective to show details of the cell structure. In vivo images were acquired with a 2° field of view yielding 256 pixels per degree. High-NA ex vivo images are summed images from a focus stack including the ganglion cell layer and the inner plexiform layer. The nerve fiber layer was excluded in the sum to increase visibility of the dendrites. The in vivo images are a registered average of 1000 raw video frames. Images have been rescaled and contrast enhanced for display purposes. Scale bars: 25 μm (**a**–**c**), 50 μm (**d**–**f**).

positional accuracy of the imaging system is a better descriptor of the imaging performance than the axial resolution. The positional accuracy of the instrument was characterized by dividing one axial through-focus data set into four interleaved segments of 250 raw frames of a total of 1000 frames. Each set was processed identically to measure the repeatability of the relative axial position of 15 ganglion cell bodies. The average SD of the axial position or the positional accuracy was 4 μm, nearly 1/30 the measured FWHM.

Analysis of the ex vivo tissue resulted in the discovery of ganglion cells displaced into the inner nuclear layer (INL) of the retina. Most cells displaced into the INL are melanopsin cells, which have been described by Berson et al.[23] and Dacey et al.[6] According to Dacey et al.,[6] 3000 of these cells are present across the retina, and 40% are displaced in the INL.[6] In the data set analyzed for the axial positional accuracy, three displaced ganglion cells were identified. Measurements from the in vivo data (Fig. 6) showed that the displaced cells could be accurately distinguished from superficial cells. The average displacement of the three cells from superficial cells was 32.2 μm, and the average SD of the displacement was 5.4 μm.

DISCUSSION

Imaging Axonal and Dendritic Structures of Ganglion Cells In Vivo

To the best of our knowledge, these data are the first demonstration of imaging of the axonal and dendritic structures of healthy primate ganglion cells in vivo. The results in this study show that AO correction, combined with in vivo fluorescence imaging, yields a significant increase in resolution, image intensity, and the image contrast of cellular structure. The resolution is fine enough that individual dendrites can be used to distinguish between some ganglion cell types in the living eye.

The application of AO to optical coherence tomography (OCT) has yielded equivalent transverse resolution to en face AO imaging techniques as well as extremely fine axial resolution (2–5 μm). To date, the best AO OCT images have revealed only hints of ganglion cells in vivo[24–26] and are limited by speckle noise inherent in the technique. Imaging submicron structures, such as dendrites and axons in vivo with OCT, is challenging because of the complicated meshwork of fine structures of similar refractive index. The advantage of fluores-

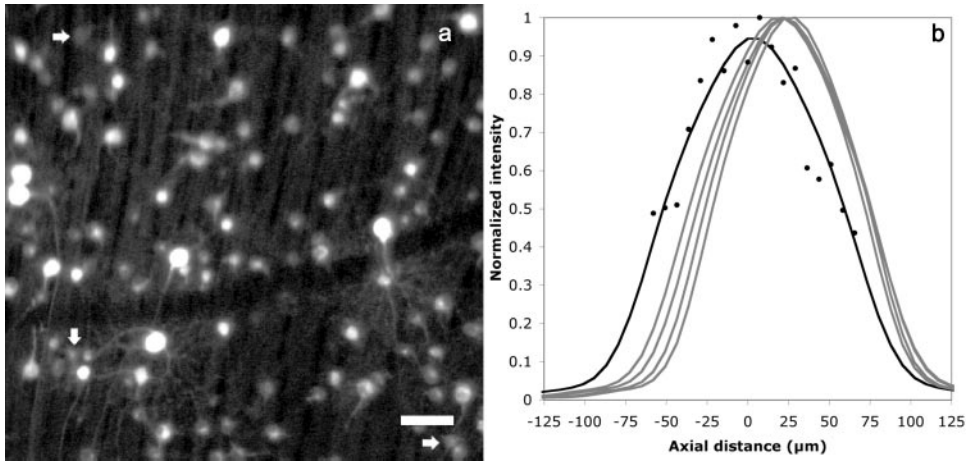

FIGURE 6. (**a**) In vivo image; *white arrows* point to the three displaced ganglion cells that were measured. Scale bar, 50 μm. (**b**) Example fit of an in vivo axial profile of a displaced ganglion cell (*black*). *Gray curves*: fits of axial profiles of four neighboring ganglion cells in the ganglion cell layer.

cence imaging is that selective dye labeling can provide high-contrast images of optically isolated structures.

The measurements of resolution presented here are, to the best of our knowledge, the first direct measurements of transverse resolution of an AO in vivo retinal imaging system. Liang et al.[1] and Zhang et al.[27] report indirect measurements of transverse resolution in AO imaging comparable to measurements presented here (1.65–2.33 μm), but those measurements were based on data from the wavefront sensor that was used to estimate the FWHM of the PSF. Romero-Borja et al.[28] reported in vivo axial resolution measurements of reflected light from a blood vessel in humans that ranged from 71 μm to 330 μm, depending on pinhole size and subject. Although these are in the same range as present measures, reflections from a blood vessel are difficult to analyze because they include a combination of diffuse and specular reflections[28] and may be influenced by strong reflections at the apex of the cylindrical blood vessel.

Our measurements of the axial positional accuracy are based on a single focus data set. Repeated measurements of the axial profile were not possible, but this may be required to fully characterize positional accuracy.

Chromatic aberration in the eye between the excitation wavelength and the broadband emission of rhodamine dye may be the most significant source of error in the axial resolution and positional accuracy measurements. The rhodamine dye emission has a peak at 590 nm and extends past both ends of the 40-nm bandwidth filter used for imaging. By linearly scaling the chromatic aberration from a human eye based on the model established by Thibos et al.[29] to reflect a greater amount of aberration for a smaller eye, the chromatic aberration across the wavelength range used corresponds to 50 μm of focus error. In scanning fluorescence imaging systems with large pinholes, the monochromatic aberrations of the excitation beam determine the transverse resolution. For excitation with a monochromatic source and collection with a large pinhole, longitudinal chromatic aberration is expected to affect only signal-to-noise, not transverse resolution, measurements.

Ganglion Cell Classification

Dendritic field diameter, axial stratification into the inner plexiform layer, and dendritic branching are the primary tools for classifying ganglion cell types. The experiments presented here demonstrate that classification of some ganglion cell types is feasible in vivo. Given the relatively poor optical sectioning, the AOSLO is best at imaging objects that are transversely separated (i.e., not directly on top of each other). As such, measurements of dendritic stratification between ON and OFF midget ganglion cells (typically between 10 and 40 μm) may be difficult. However, dendrite stratification in which objects are transversely isolated may be measured by improving the positional accuracy to less than 4 μm through increased averaging. Additionally, by taking advantage of the known properties of the connectivity of different classes of ganglion cells in the LGN, a priori knowledge of which ganglion types are labeled would facilitate in vivo classification.[30]

Many of the displaced cells we imaged and distinguished from superficial cells may be melanopsin-containing cells, a recently discovered type of ganglion cell thought to have a role in the circadian rhythm, contribute to the pupillary reflex, and convey information about ambient light conditions.[6,23] This in vivo method may be a way to further investigate the functional role of these cell types and their role in retinal disease through direct visualization in a live animal.

Future Applications

The ability to visualize individual ganglion cell axonal and dendritic structures is a powerful tool allowing the investigation of early cellular changes in retinal disease in vivo. For instance, with the same imaging system used in this study, individual primate retinal pigment epithelial cells using lipofuscin autofluoresce, recently presented by Morgan et al. (*IOVS* 2007;48:ARVO E-Abstract 1953), has revealed fine structures such as RPE cell nuclei and lipofuscin granules.

An important use for this in vivo imaging method is to examine dendritic processes in primate retinal ganglion cells during the progression of eye disease (e.g., in a macaque model of glaucoma). We are testing new approaches to labeling ganglion cells that avoid the phototoxicity and transitory labeling of rhodamine dye, such as genetic labeling of ganglion cells with green fluorescence protein (GFP), as demonstrated in primate photoreceptors by Mancuso et al.[31] In vivo imaging can also be used to image retinal cells that naturally contain fluorescent species, such as RPE cells, as mentioned, or melanopsin-containing retinal ganglion cells (Dacey DM, personal communication, March 2005). This would permit investigation of several retinal cell types in the normal retina and could also be used to investigate cellular remodeling before, during, and after cellular apoptosis in retinal disease in a live animal, as is being explored ex vivo by Marc et al.,[32–36] Morgan et al.,[37] and Datta et al. (*IOVS* 2005;46:ARVO E-Abstract 1233).

In future studies, AO can be combined with developments in molecular biology (e.g., development of optical switches by which ganglion cells could be turned off) to permit study of the functional role of ganglion cells in vision.[38] Use of additional tools to label retinal ganglion cells, such as transfection of retinal ganglion cells with voltage-sensitive dyes, combined with in vivo fluorescence imaging, would supplement standard electrophysiological investigations in understanding ganglion cell electrical response to light.

References

1. Liang J, Williams DR, Miller D. Supernormal vision and high-resolution retinal imaging through adaptive optics. *J Opt Soc Am A*. 1997;14:2884–2892.
2. Roorda A, Romero-Borja F, Donnelly WJ, Queener H, Hebert TJ, Campbell MCW. Adaptive optics scanning laser ophthalmoscopy. *Opt Express*. 2002;10:405–412.
3. Hermann B, Fernandez EJ, Unterhuber A, et al. Adaptive-optics ultrahigh-resolution optical coherence tomography. *Opt Lett*. 2004;29:2142–2144.
4. Rodieck RW, Watanabe M. Survey of the morphology of macaque retinal ganglion-cells that project to the pretectum, superior colliculus, and parvicellular laminae of the lateral geniculate-nucleus. *J Comp Neurol*. 1993;338:289–303.
5. Watanabe M, Rodieck RW. Parasol and midget ganglion-cells of the primate retina. *J Comp Neurol*. 1989;289:434–454.
6. Dacey DM, Liao HW, Peterson BB, et al. Melanopsin-expressing ganglion cells in primate retina signal colour and irradiance and project to the LGN. *Nature*. 2005;433:749–754.
7. Dacey DM, Peterson BB, Robinson FR, Gamlin PD. Fireworks in the primate retina: in vitro photodynamics reveals diverse LGN-projecting ganglion cell types. *Neuron*. 2003;37:15–27.
8. Dacey DM, Lee BB. The blue-ON opponent pathway in primate retina originates from a distinct bistratified ganglion cell type. *Nature*. 1994;367:731–735.
9. Dacey DM. The mosaic of midget ganglion-cells in the human retina. *J Neurosci*. 1993;13:5334–5355.
10. Merigan WH, Katz LM, Maunsell JHR. The effects of parvocellular lateral geniculate lesions on the acuity and contrast sensitivity of macaque monkeys. *J Neurosci*. 1991;11:994–1001.
11. Cordeiro MF, Guo L, Luong V, et al. Real-time imaging of single nerve cell apoptosis in retinal neurodegeneration. *Proc Natl Acad Sci USA*. 2004;101:13352–13356.
12. Gray DC, Merigan W, Wolfing JI, et al. In vivo fluorescence imaging of primate retinal ganglion cells and retinal pigment epithelial cells. *Opt Express*. 2006;14:7144–7158.

13. Higashide T, Kawaguchi I, Ohkubo S, Takeda H, Sugiyama K. In vivo imaging and counting of rat retinal ganglion cells using a scanning laser ophthalmoscope. *Invest Ophthalmol Vis Sci*. 2006; 47:2943–2950.
14. Paques M, Sirnonutti M, Roux MJ, et al. High resolution fundus imaging by confocal scanning laser ophthalmoscopy in the mouse. *Vision Res*. 2006;46:1336–1345.
15. Thanos S, Indorf L, Naskar R. In vivo FM: using conventional fluorescence microscopy to monitor retinal neuronal death in vivo. *Trends Neurosci*. 2002;25:441–444.
16. Sabel BA, Engelmann R, Humphrey MF. In vivo confocal neuroimaging (ICON) of CNS neurons. *Nat Med*. 1997;3:244–247.
17. Rousseau V, Engelmann R, Sabel BA. Restoration of vision, III: soma swelling dynamics predicts neuronal death or survival after optic nerve crush in vivo. *Neuroreport*. 1999;10:3387–3391.
18. Biss DP, Sumorok D, Burns SA, et al. In vivo fluorescent imaging of the mouse retina using adaptive optics. *Opt Lett*. 2007;32:659–661.
19. Thevenaz P, Ruttimann UE, Unser M. A pyramid approach to subpixel registration based on intensity. *IEEE T Image Process*. 1998;7:27–41.
20. Wilson T. Optical sectioning in confocal fluorescent microscopes. *J Microsc-Oxford*. 1989;154:143–156.
21. Wilson T. 3-Dimensional imaging in confocal systems. *J Microsc-Oxford*. 1989;153:161–169.
22. Zucker RM. Quality assessment of confocal microscopy slide based systems: performance. *Cytometry Part A*. 2006;69A:659–676.
23. Berson DM. Strange vision: ganglion cells as circadian photoreceptors. *Trends Neurosci*. 2003;26:314–320.
24. Zhang Y, Cense B, Rha J, et al. High-speed volumetric imaging of cone photoreceptors with adaptive optics spectral-domain optical coherence tomography. *Opt Express*. 2006;14:4380–4394.
25. Zawadzki RJ, Choi S, Jones SM, Olivier SS, Werner JS. Adaptive optics-optical coherence tomography: optimizing visualization of microscopic retinal structures in three dimensions. *J Opt Soc Am A*. 2007;24:1373–1383.
26. Fernandez EJ, Povazay B, Hermann B, et al. Three-dimensional adaptive optics ultrahigh-resolution optical coherence tomography using a liquid crystal spatial light modulator. *Vision Res*. 2005;45:3432–3444.
27. Zhang YH, Roorda A. Evaluating the lateral resolution of the adaptive optics scanning laser ophthalmoscope. *J Biomed Opt*. 2006; 11:014002.
28. Romero-Borja F, Venkateswaran K, Roorda A, Hebert T. Optical slicing of human retinal tissue in vivo with the adaptive optics scanning laser ophthalmoscope. *Appl Opt*. 2005;44:4032–4040.
29. Thibos LN, Ye M, Zhang XX, Bradley A. The chromatic eye—a new reduced-eye model of ocular chromatic aberration in humans. *Appl Opt*. 1992;31:3594–3600.
30. Leventhal G, Rodieck RW, Dreher B. Retinal ganglion-cell classes in the old-world monkey—morphology and central projections. *Science*. 1981;213:1139–1142.
31. Mancuso K, Hendrickson AE, Connor TBJ, et al. Recombinant adeno-associated virus targets passenger gene expression to cones in primate retina. *J Opt Soc Am A*. 2007;24:1411–1416.
32. Jones BW, Marc RE. Retinal remodeling during retinal degeneration. *Exp Eye Res*. 2005;81:123–137.
33. Marc RE, Jones BW, Lucas RJ. Excitatory self-signaling in retinal remodeling. *Invest Ophthalmol Vis Sci*. 2004;45:U347–U347.
34. Watt CB, Jones BW, Yang J, Marc RE, LaVail MM. Complex rewiring in retinal remodeling. *Invest Ophthalmol Vis Sci*. 2004;45: U336–U336.
35. Jones BW, Watt CB, Vaughan DK, Organisciak DT, Marc RE. Retinal remodeling triggered by light damage in the albino rat. *Invest Ophthalmol Vis Sci*. 2003;44:U715–U715.
36. Marc RE, Jones BW. Retinal remodeling in inherited photoreceptor degenerations. *Mol Neurobiol*. 2003;28:139–147.
37. Morgan JE, Datta AV, Erichsen JT, Albon J, Boulton ME. Retinal ganglion cell remodeling in experimental glaucoma. *Adv Exp Med Biol*. 2006;572:397–402.
38. Banghart M, Borges K, Isacoff E, Trauner D, Kramer RH. Light-activated ion channels for remote control of neuronal firing. *Nat Neurosci*. 2004;7:1381–1386.